 doi:10.20944/preprints201912.0091.v1

Article

A Modified Cell-Based Strain Smoothing for Material Nonlinearity

Changkye Lee [1] and Sundararajan Natarajan [2]*

[1] University Core Research Center for Disaster-free and Safe Ocean City Construction, Dong-A University, 49315, Busan, Korea; changkyelee@dau.ac.kr (C.L.)
[2] Integrated Modelling Simulation Lab, Department of Mechanical Engineering, Indian Institute of Technology Madras, 600036, Chennai, India
* Correspondence: snatarajan@iitm.ac.in; Tel. +91-44-2257-4656

Abstract: This work presents a linear smoothing scheme over high-order triangular elements in the framework of a cell-based strain smoothed finite element method for two-dimensional nonlinear problems. The main idea behind the proposed linear smoothing scheme for strain-smoothed finite element method (S-FEM) is no subdivision of finite element cells to sub-cells while the classical S-FEM needs sub-cells. Since the linear smoothing function is employed, S-FEM is able to use quadratic triangular or quadrilateral elements. The modified smoothed matrix obtained node-wise is evaluated. In the same manner with the computation of the strain-displacement matrix, the smoothed stiffness matrix and deformation graident are obtained over smoothing domains. A series of benchmark tests are investigated to demonstrate validity and stability of the proposed scheme. The validity and accuracy are confirmed by comparing the obtained numerical results with the standard FEM using 2nd-order triangular element and the exact solutions.

Keywords: Cell-based smoothed finite element method; quadratic triangular element; linear smoothing function; hyperelasticity

---

1. Introduction

A strain smoothing approach in the framework of finite element approximation (S-FEM) was introduced to handle the known difficulties of simple finite elements, which are prone to locking and highly sensitive to heavily distorted meshes ([1,2]). These limits often harm the accuracy and stability of finite element method (FEM) results when nearly- and full-incompressible material problems are considered. Since Liu et al. [3] introduced four different S-FEM approaches, i.e. cell-based S-FEM (CS-FEM), edge-based S-FEM (ES-FEM), node-based S-FEM (NS-FEM) and face-based S-FEM (FS-FEM),

Preprints (www.preprints.org) | NOT PEER-REVIEWED | Posted: 7 December 2019 doi:10.20944/preprints201912.0091.v1

several approaches have been widely used in various engineering fields: plate (Nguyen-Xuan et al. [4]), shell (Nguyen-Thanh et al. [5]), nearly-incompressible elasticity (Lee et al. [6] and Ong et al. [7]), and coupled with extended FEM (Bordas et al. [8,9]). Moreover, selective S-FEM [10], the hybrid S-FEM [11] and enriched-S-FEM [6] were introduced to improve conventional S-FEMs.

Among various S-FEMs, CS-FEM provides an almost identical accuracy as FEM with simple elements. However, Natarajan et al. [12] found that cell-based strain smoothing approach over arbitrary polytopes resulted in less accuracy than FEM for polygonal elements. Francis et al. [13] introduced modified linear smoothing in cell-based smoothed-strain scheme for arbitrary polygonal cells and showed improved accuracy and convergence.

In their work, the modified cell-based linear smoothing scheme was employed by dividing the arbitrary polygons into triangular/tetrahedral sub-cells where the stiffness matrix is calculated. The transformation of quadratic serendipity shape functions introduced by Rand et al. [14] was used to obtain shape functions for polygonal cells. Wachspress rational basis functions for polygons were chosen as the barycentric shape functions where the functions are converted into serendipity shape functions that satisfies the Lagrange property.

In the present work, the linear smoothing scheme was employed for the quadratic triangular element. Unlike the cell-based linear smoothing scheme for arbitrary polytopes or the standard CS-FEM, the proposed approach does not need to divide finite element cells into sub-cells. Namely, quadratic triangular cells are target cells and smoothing domains; thus no further intervention to construct sub-cells is needed. The linear polynomial basis function is selected as the linear smoothing function for CS-FEM whereas the conventional CS-FEM has the constant linear smoothing function. Using the smoothing function, the modified shape functions are computed and the node-wise modified strain-displacement are evaluated over each smoothing domain.

In Section 2 of this paper, cell-based strain smoothing approach in nonlinear approximation is briefly revisited. In the subsequent section, the linear smoothing function in the context of CS-FEM is introduced, which illustrated the computation of the strain-displacement matrix. In Section 4, several numerical tests are studied to validate the proposed method in quasi-incompressible limits (Poisson's ratio). In the final section, the performance of the proposed method was conclude and some possible future works were prawn related to the present method.

2. Method

2.1. Nonlinear cell-based smoothed finite element method approximation

In this section, the basic idea behind cell-based-smoothed strain finite element method (CS-FEM) is briefly introduced (Liu and Nguyen [3]). The main features of CS-FEM are the subdivision of a finite

 doi:10.20944/preprints201912.0091.v1

element cell and numerical integration. In CS-FEM, a finite element is divided into three sub-cells that called a smoothing domain as shown in Figure 1. Over the smoothing domain, the strain-displacement and the stiffness matrices are constructed, viz. strains and stresses are smoothed on smoothing domain, and not on an element.

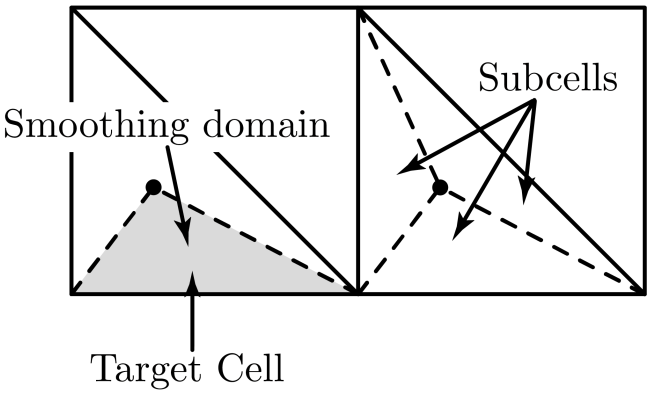

Figure 1. The subdivision of a finite element cell into sub-cells and construction of smoothing domain in CS-FEM.

Another distinguished feature is the numerical integration. In strain-smoothing approach, the numerical integration performs on the boundaries of smoothing domains as the line integration while it performs in the element in FEM. Note that since the numerical integration is performed globally in the proposed method, the Jacobian matrix is not required. To compute the strain-displacement matrix, one Gauss point on the middle of the boundary of smoothing domain and outward normal vectors are used. Figure 2 illustrates the integration scheme in CS-FEM with the location of Gauss points and outward normal vectors.

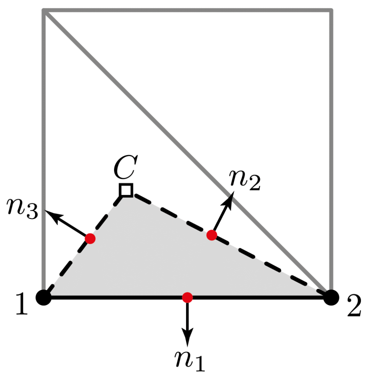

Figure 2. The numerical integration of the strain smoothing method. Sub-cell △12C is smoothing domain of CS-FEM. White square C is a centroid of the element and black circles are element nodes. Red circles are Gauss points located on the mid-point of the boundary of smoothing domain. Black arrows are the outward normal vectors at Gauss points.

For the nonlinear CS-FEM approximation, the following smoothed infinitesimal strain tensor over smoothing domain Ω is given as [6]:

Preprints (www.preprints.org) | NOT PEER-REVIEWED | Posted: 7 December 2019 doi:10.20944/preprints201912.0091.v1

$$\forall \mathbf{x} \in \Omega_k^s, \quad \bar{\varepsilon}^{\mathrm{h}}\left(\mathbf{x}_k\right) = \int_{\Omega_k^s} \varepsilon^{\mathrm{h}}\left(\mathbf{x}\right) \Phi\left(\mathbf{x}\right) \mathrm{d}\Omega, \tag{1}$$

where a point $\mathbf{x}_k$ is located in smoothing domain and $\Phi\left(\mathbf{x}\right)$ is the weight function. Using the divergence theorem, the smoothed strain can be rewritten as:

$$\bar{\varepsilon}^{\mathrm{h}} = \frac{1}{A_k^s} \int_{\Omega_k^s} \varepsilon^{\mathrm{h}}\left(\mathbf{x}\right) \mathrm{d}\Omega = \frac{1}{A_k^s} \int_{\Gamma_k^s} \mathbf{n}\left(\mathbf{x}\right) \mathbf{u}^{\mathrm{h}}\left(\mathbf{x}\right) \mathrm{d}\Gamma, \tag{2}$$

where A_k^s is the area of smoothing domain, Γ_k^s is the boundary of smoothing domain and n is the outward normal vector in the form of the following matrix in two dimensions:

$$\mathbf{n}\left(\mathbf{x}\right) = \begin{bmatrix} n_1 & 0 \\ 0 & n_2 \\ n_2 & n_1 \end{bmatrix}. \tag{3}$$

The details of the method are given by Lee [15]. However, brief information of the smoothed Galerkin weak form and its linearization is given as follows:

$$\int_{\Omega} \frac{\partial W}{\partial \bar{\mathbf{F}}}\left(\mathbf{X}, \bar{\mathbf{F}}\left(\mathbf{u}\right)\right) : \nabla \mathbf{v} \mathrm{d}\Omega = \int_{\Omega} \mathbf{f} \cdot \mathbf{v} \mathrm{d}\Gamma + \int_{\Gamma_N} \mathbf{g} \cdot \mathbf{v} \mathrm{d}\Gamma, \tag{4}$$

where $\mathbf{v}$ is the set of admissible test function and $\mathbf{F}$ is the smoothed deformation gradient evaluated over each smoothing domain. Equation (4) can be expressed with the energy function $\mathcal{R}\left(\mathbf{u}\right)$ and its directional derivatives $D\mathcal{R}\left(\mathbf{u}\right) \cdot \mathbf{u}$:

$$\mathcal{R}\left(\mathbf{u}\right) = \int_{\Omega} \frac{\partial W}{\partial \bar{\mathbf{F}}_{ij}}\left(\mathbf{X}, \bar{\mathbf{F}}\left(\mathbf{u}\right)\right) \frac{\partial v_i}{\partial X_j} \mathrm{d}\Omega - \int_{\Omega} f_i v_i \mathrm{d}\Omega + \int_{\Gamma_N} g_i v_i \mathrm{d}\Gamma, \tag{5}$$

$$D\mathcal{R}\left(\mathbf{u}\right) \cdot \mathbf{u} = \int_{\Omega} \frac{\partial^2 W}{\partial \bar{\mathbf{F}}_{ij} \partial \bar{\mathbf{F}}_{kl}}\left(\mathbf{X}, \bar{\mathbf{F}}\left(\mathbf{u}\right)\right) \frac{\partial v_i}{\partial X_j} \mathrm{d}\Omega, \tag{6}$$

where $i, j, k, l \in \{1, 2\}$ for tow dimension and W is the stored strain energy function.

To find an approximate solution to Equation (4), the Newton-Raphson iterative method is employed. At iteration iter $+ 1$, knowing the displacement $\mathbf{u}_{\mathrm{iter}}$ from iteration iter, find $\mathbf{r}$ iter that satisfies:

$$D\mathcal{R}\left(\mathbf{u}_{\mathrm{iter}}\right) \cdot \mathbf{r}_{\mathrm{iter}} = -\mathcal{R}\left(\mathbf{u}_{\mathrm{iter}}\right). \tag{7}$$

Therefore Equations (5) and (6) can be rewritten as follows:

Preprints (www.preprints.org) | NOT PEER-REVIEWED | Posted: 7 December 2019 doi:10.20944/preprints201912.0091.v1

$$\mathcal{R}\left(\mathbf{u}\right)=\int_{\Omega}2\frac{\partial W}{\partial \bar{C}_{ij}}\bar{\mathbf{F}}_{ki}\frac{\partial v_k}{\partial X_j}\mathrm{d}\Omega-\int_{\Omega}f_i v_i \mathrm{d}\Omega+\int_{\Gamma_N}g_i v_i \mathrm{d}\Gamma, \tag{8}$$

and

$$D\mathcal{R}\left(\mathbf{u}\right)\cdot\mathbf{r}=\int_{\Omega}\left(\frac{\partial^2 W}{\partial \bar{C}_{ij}\partial \bar{C}_{kl}}\bar{F}_{pi}\frac{\partial v_p}{\partial X_j}\bar{F}_{sk}\frac{\partial v_s}{\partial X_l}+2\frac{\partial W}{\partial \bar{C}_{ij}}\frac{\partial r_k}{\partial X_i}\frac{\partial v_k}{\partial X_j}\right)\mathrm{d}\Omega, \tag{9}$$

where $\bar{\mathbf{C}}$ is the smoothed right Cauchy-Green deformation $\bar{\mathbf{C}}=\bar{\mathbf{F}}^{\mathrm{T}}\bar{\mathbf{F}}$.

The global system of equations at each iteration can be written as:

$$\bar{\mathbf{K}}_{\text{iter}}\mathbf{r}_{\text{iter}}=\bar{\mathbf{b}}_{\text{iter}}, \tag{10}$$

thus, the displacement $\mathbf{u}$ is obtained by the iteration method: $\bar{\mathbf{u}}_{\text{iter}+1}=\bar{\mathbf{u}}_{\text{iter}}+\mathbf{r}_{\text{iter}}$.

2.2. Linear smoothing function in the framework of CS-FEM approximation

In the conventional strain smoothing method, the smoothing function f is a constant, that is $f\left(x\right)=1$. This smoothing function is suitable for the strain smoothing approach with linear quadrilateral or triangular elements. However, when the quadratic elements are used in S-FEM, the given smoothing function cannot be used (Francis et al. [13]). Therefore, to use quadratic elements, the following linear polynomial basis is chosen as the linear smoothing function:

$$f\left(x\right)=\left[\begin{array}{ccc}0 & x_1 & x_2\end{array}\right], \tag{11}$$

and its derivative is $f_{,j}\left(x\right)=\left[\begin{array}{ccc}0 & \delta_{1j} & \delta_{2j}\end{array}\right]^{\mathrm{T}}$.

The right hand side of Equation (1) with the smoothing function would yield the basis function derivatives level, which can be expressed as follows:

$$\int_{\Omega_k^s}\Psi_{a,j}f\left(x\right)\mathrm{d}\Omega=\int_{\Gamma_k^s}\Psi_a f\left(x\right)n_j \mathrm{d}\Gamma-\int_{\Omega_k^s}\Psi_a f_{,j}\left(x\right)\mathrm{d}\Omega, \tag{12}$$

where Ψ is the set of the shape functions. Note that in this work, Lagrange basis functions are used as shape functions. For two dimensional problems, Equation (12) with the linear smoothing function (see Equation (11)) can be expanded as follows:

 doi:10.20944/preprints201912.0091.v1

$$
\begin{aligned}
\int_{\Omega_k^s} \Psi_{a,1} f(x)\, \mathrm{d}\Omega &= \int_{\Gamma_k^s} \Psi_a n_1 \mathrm{d}\Gamma \\
\int_{\Omega_k^s} \Psi_{a,1} x_1 \mathrm{d}\Omega &= \int_{\Gamma_k^s} \Psi_a x_1 n_1 \mathrm{d}\Gamma - \int_{\Omega_k^s} \Psi_a \mathrm{d}\Omega \\
\int_{\Omega_k^s} \Psi_{a,1} x_2 \mathrm{d}\Omega &= \int_{\Gamma_k^s} \Psi_a x_2 n_1 \mathrm{d}\Gamma,
\end{aligned}
\tag{13}
$$

and

$$
\begin{aligned}
\int_{\Omega_k^s} \Psi_{a,2} f(x)\, \mathrm{d}\Omega &= \int_{\Gamma_k^s} \Psi_a n_2 \mathrm{d}\Gamma \\
\int_{\Omega_k^s} \Psi_{a,2} x_1 \mathrm{d}\Omega &= \int_{\Gamma_k^s} \Psi_a x_1 n_2 \mathrm{d}\Gamma \\
\int_{\Omega_k^s} \Psi_{a,2} x_2 \mathrm{d}\Omega &= \int_{\Gamma_k^s} \Psi_a x_2 n_2 \mathrm{d}\Gamma - \int_{\Omega_k^s} \Psi_a \mathrm{d}\Omega,
\end{aligned}
\tag{14}
$$

for $\Psi_{a,1}$ and $\Psi_{a,2}$, respectively.

The cell-based smoothing domains are also used for the numerical integration for Equations (13) and (14). Figure 3 shows the numerical integration scheme for the proposed cell-based strain-smoothed method. In the proposed method, the finite element cell does not require to be divided into sub-cells as the conventional CS-FEM. Namely, the finite element cell is the target cell and smoothing domain in this case.

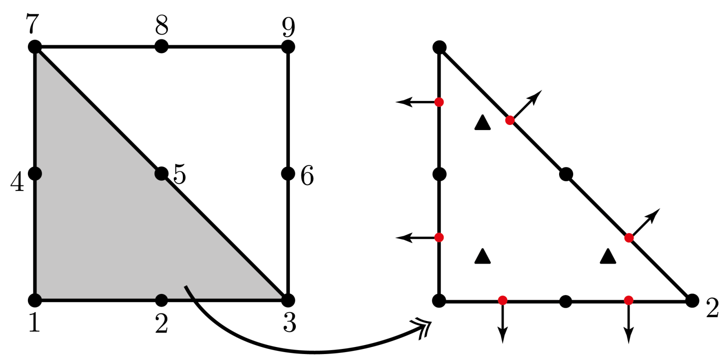

Figure 3. The construction of smoothing domain and numerical scheme in CS-FEM with the linear smoothing function for the quadratic triangular mesh. The interior Gauss points are black triangles while Gauss points on the boundaries are red circles. The outward normal vectors are depicted as black arrows.

Another feature that can be found in Figure 3 is the number of Gauss points. The proposed scheme has two different Gauss point locations: first location can be found on the boundaries of smoothing domains and another is the interior Gauss points. Three interior Gauss points and two Gauss points

Preprints (www.preprints.org) | NOT PEER-REVIEWED | Posted: 7 December 2019 doi:10.20944/preprints201912.0091.v1

on the boundaries are required to compute for the smoothed stiffness matrix. Therefore, the following system of equations is applied to evaluate the smoothed strain-displacement matrix:

$$\mathbf{W}d_j = f_j, \quad j \in \{1,2\}\,, \tag{15}$$

where

$$\mathbf{W} = \begin{bmatrix} {}^1W & {}^2W & {}^3W \\ {}^1W\,{}^1x_1 & {}^2W\,{}^2x_1 & {}^3W\,{}^3x_1 \\ {}^1W\,{}^1x_2 & {}^2W\,{}^2x_2 & {}^3W\,{}^3x_2 \end{bmatrix}, \tag{16}$$

$$\begin{aligned} f_1 &= \begin{bmatrix} \sum\limits_{k=1}^{3}\sum\limits_{g=1}^{2} \Psi_a\left({}^g_k s\right)\, {}_k n_1\, {}^g_k v \\ \sum\limits_{k=1}^{3}\sum\limits_{g=1}^{3} \Psi_a\left({}^g_k s\right) {}^g_k s_1\, {}_k n_1\, {}^g_k v - \sum\limits_{m=1}^{3} \Psi_a\left({}^m r\right) {}^m w \\ \sum\limits_{k=1}^{3}\sum\limits_{g=1}^{2} \Psi_a\left({}^g_k s\right) {}^g_k s_2\, {}_k n_1\, {}^g_k v \end{bmatrix} \\ f_2 &= \begin{bmatrix} \sum\limits_{k=1}^{3}\sum\limits_{g=1}^{2} \Psi_a\left({}^g_k s\right)\, {}_k n_2\, {}^g_k v \\ \sum\limits_{k=1}^{3}\sum\limits_{g=1}^{3} \Psi_a\left({}^g_k s\right) {}^g_k s_1\, {}_k n_2\, {}^g_k v \\ \sum\limits_{k=1}^{3}\sum\limits_{g=1}^{2} \Psi_a\left({}^g_k s\right) {}^g_k s_2\, {}_k n_2\, {}^g_k v - \sum\limits_{m=1}^{3} \Psi_a\left({}^m r\right) {}^m w \end{bmatrix}, \end{aligned} \tag{17}$$

and

$$d_j = \begin{bmatrix} {}^1d_j & {}^2d_j & {}^3d_j \end{bmatrix}^{\mathrm{T}} = \begin{bmatrix} \Psi_{a,j}\left({}^1r\right) & \Psi_{a,j}\left({}^2r\right) & \Psi_{a,j}\left({}^3r\right) \end{bmatrix}^{\mathrm{T}}. \tag{18}$$

The coordinates of the m^{th} interior Gauss points are defined as ${}^m r = ({}^m r_1, {}^m r_2)$ and their weights are given as ${}^m w$. On the other hand, the coordinates of g^{th} Gauss points ${}^g_k s = \left({}^g_k s_1, {}^g_k s_2\right)$ and their weights ${}^g_k v$ are given at the k^{th} boundaries of smoothing domain. The outward normal at the k^{th} boundary of smoothing domain is given as ${}_k\mathrm{n} = ({}_k n_1, {}_k n_2)$. Equation (18) denotes the solution vector of Equation (15). The j^{th} basis function derivatives are obtained at the three interior Gauss points in each smoothing domain (Figure 3). Using the obtained solution vector, the modified smoothed strain-displacement matrix can be obtained:

$$\bar{\mathbf{B}}\left({}^k\mathbf{r}\right) = \begin{bmatrix} \bar{B}_1\left({}^k\mathbf{r}\right) & \bar{B}_2\left({}^k\mathbf{r}\right) & \cdots & \bar{B}_n\left({}^k\mathbf{r}\right) \end{bmatrix}, \quad k \in \{1,2,3\}\,, \tag{19}$$

where the nodal strain-displacement matrix evaluated at the k^{th} interior Gauss points is expressed as:

 doi:10.20944/preprints201912.0091.v1

$$\bar{B}_a\left({}^k\mathbf{r}\right) = \begin{bmatrix} {}^kd_1 & 0 \\ 0 & {}^kd_2 \\ {}^kd_2 & {}^kd_1 \end{bmatrix}. \tag{20}$$

3. Results

In this section, the validity and stability of the proposed linear smoothing function for the quadratic triangular elements in nonlinear problems are demonstrated. The following series of benchmark tests are studied: 1) simple shear deformation with Dirichlet and mixed Dirichlet and Neumann boundary conditions (BCs), 2) uniform extension with lateral contraction with Dirichlet and mixed Dirichlet and Neumann BCs, 3) "Not-so-simple" shear deformation with Dirichlet BCs and 4) bending of a rectangular block with Dirichlet BCs.

For nonlinearity, a neo-Hookean hyperelastic model is used [16]:

$$W = \frac{1}{2}\left(\ln J\right)^2 - \mu \ln J + \frac{1}{2}\mu\left(\mathrm{tr}\mathbf{C} - 3\right), \tag{21}$$

where Lamé's first parameter $\lambda = \kappa - (1/2)\,\mu$ is defined using the shear modulus μ and bulk modulus κ in two dimensions. The Jacobian is given as $J = \det\mathbf{F}$. The present CS-FEM is compared with the exact solutions and quadratic triangular elements in FEM. The details of numerical tests, i.e. implementation of boundary conditions and exact solutions in strain energy can be found in References [6] and [15]. Note that benchmark tests are considered as the dimensionless.

3.1. Discussion

3.1.1. Simple shear deformation

First, simple shear deformation with two different types of boundary conditions are considered: 1) Dirichet BCs and 2) mixed Dirichlet and Neumann BCs. Figure 4 depicts the initial and deformed shapes of the unit square for the problem.

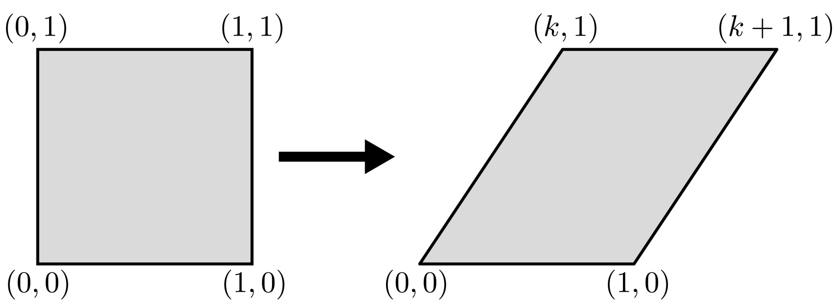

Figure 4. Initial and deformed shapes of simple shear deformation with Dirichlet boundary conditions.

To impose Dirichlet and Neumann BCs for simple shear deformation, the following deformation gradient and first Piola-Kirchhoff stress tensor are defined, respectively:

$$\mathbf{F} = \begin{bmatrix} 1 & k & 0 \\ 0 & 1 & 0 \\ 0 & 0 & 1 \end{bmatrix}, \tag{22}$$

and

$$\mathbf{P} = \begin{bmatrix} 0 & k\mu & 0 \\ k\mu & 0 & 0 \\ 0 & 0 & 0 \end{bmatrix}, \tag{23}$$

where $k > 0$ and its strain energy using Equation (21) is given as:

$$\mathrm{W} = \frac{\mu}{2}k^2. \tag{24}$$

The present work uses $k = 1$ for the deformation gradient. To compute the strain energy, the shear modulus $\mu = 0.6$ and bulk modulus $\kappa = 100$ are used, which is equivalent to Poisson's ratio $\nu = 0.497$. Hence, the strain energy for simple shear deformation is determined to be $\mathrm{W} = 0.3$. Tables 1 and 2 provide the detailed values of displacement relative error for FEM and proposed CS-FEM with the quadratic 6-node node triangular (T6) element. It can be found that the proposed method shows the exact solution down to machine precision.

Table 1. Displacement relative error ($\times 10^{-12}$) for simple shear deformation with Dirichlet BCs.

DOFs	FEM with T6	CS-FEM with T6
50	0.00057	0.10846
162	0.00144	0.15607
338	0.00185	0.01571
578	0.00199	0.14690
880	0.00214	0.14206

Table 2. Displacement relative error ($\times 10^{-12}$) for simple shear deformation with Dirichlet and Neumann BCs.

DOFs	FEM with T6	CS-FEM with T6
50	0.10186	0.13922
162	0.10172	0.14249
338	0.10038	0.13953
578	0.09941	0.13973
880	0.09647	0.14025

Preprints (www.preprints.org) | NOT PEER-REVIEWED | Posted: 7 December 2019 doi:10.20944/preprints201912.0091.v1

3.1.2. Uniform extension with lateral contraction

The next test is uniform extension with lateral contraction using Dirichlet and mixed Dirichlet and Neumann BCs. The geometry and material properties used are the same as the simple shear deformation. The deformation gradient and non-zero components of the first Piola-Kirchhoff stress tensor are:

$$\mathbf{F} = \begin{bmatrix} \lambda_1 & 0 & 0 \\ 0 & \lambda_2 & 0 \\ 0 & 0 & \lambda_2 \end{bmatrix}, \tag{25}$$

and

$$P_{11} = \frac{\sigma_{11}}{\lambda_1} = \mu\left(\lambda_1 - \frac{1}{\lambda_1}\right) = -P_{22}, \tag{26}$$

where $\lambda_1 = 1.15$, $\lambda_2 = 1/\lambda_1$ and $\lambda_3 = 1$. Hence $P_{11} = -P_{22} = 0.16826087$ and the strain energy is $\mathrm{W} = \frac{\mu}{2}\left(\lambda_1^2 + \frac{1}{\lambda_1^2} - 2\right) \approx 0.02359$.

Figures 5 and 6 illustrate the deformed shapes of uniform extension with lateral contraction using Dirichlet and mixed Dirichlet and Neumann BCs, respectively. Figure 7 shows the convergence of the displacement relative errors of FEM and proposed CS-FEM with linear smoothing for the problem with Dirichlet and mixed Dirichlet and Neumann BCs. As shown in Figure 7, a fraction is within machine precision with portion 10^{-14} for FEM and 10^{-12} for the present method.

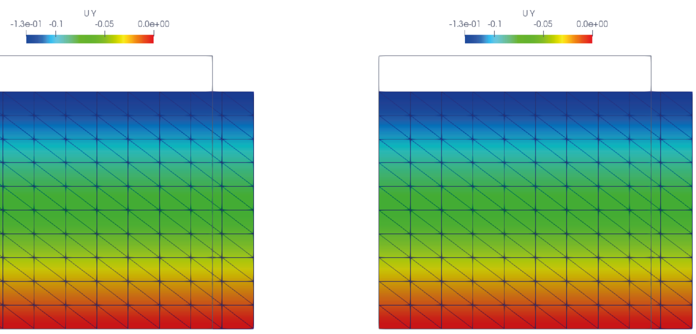

(a) FEM (b) CS-FEM

Figure 5. Deformed shapes of uniform extension with lateral contraction with Dirichlet BCs: (**a**) FEM with T6. (**b**) the proposed CS-FEM with T6.

Preprints (www.preprints.org) | NOT PEER-REVIEWED | Posted: 7 December 2019 doi:10.20944/preprints201912.0091.v1

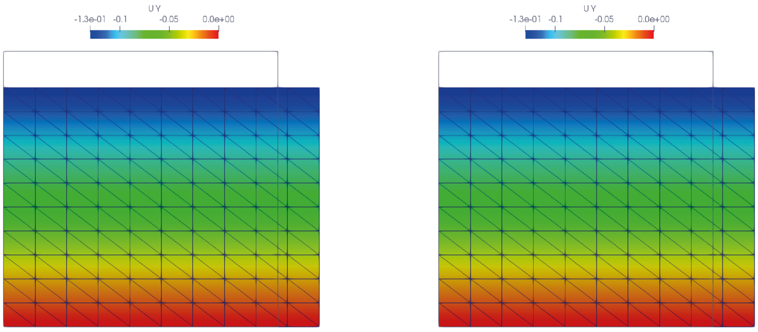

(a) FEM (b) CS-FEM

Figure 6. Deformed shapes of uniform extension with lateral contraction with mixed Dirichlet and Neumann BCs: (**a**) FEM with T6. (**b**) the proposed CS-FEM with T6.

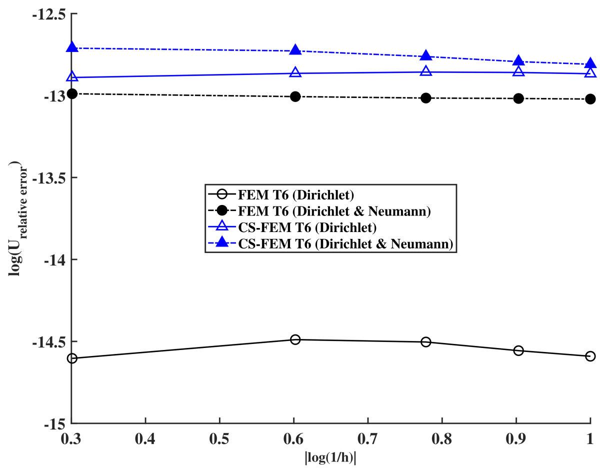

Figure 7. Convergence of the displacement relative errors of FEM and CS-FEM for uniform extension with lateral contraction with Dirichlet and mixed Dirichlet and Neumann BCs.

160 3.1.3. "Not-so-simple" shear deformation

161 This test is a non-homogeneous deformation example known as "Not-so-simple" shear
162 deformation with Dirichlet BCs. As shown in Figure 8, the geometry of this problem is $(0,2) \times (0,2)$
163 and its deformation gradient is given in Equation (27).

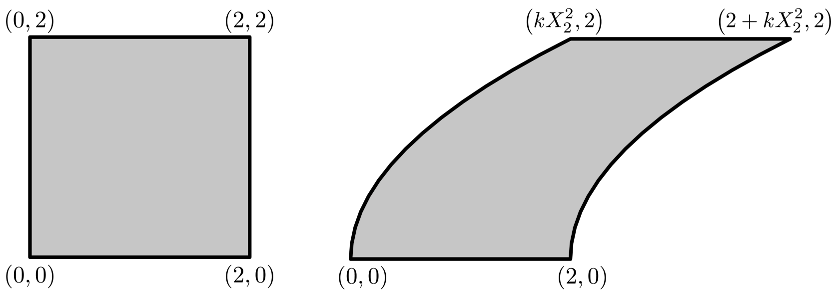

Figure 8. The geometry and deformations of "Not-so-simple" shear deformation.

$$\mathbf{F} = \begin{bmatrix} 1 & 2kX_2 & 0 \\ 0 & 1 & 0 \\ 0 & 0 & 1 \end{bmatrix}, \tag{27}$$

where $k > 1$. The exact solution in strain energy is given as $W = \frac{\mu}{2}(2kX_2)^2 = 2\mu k^2 X_2^2 = 1.6$ since the shear and bulk moduli are the same as simple shear deformation.

Figure 9 depicts the deformed shapes of "Not-so-simple" shear deformation with Dirichlet BCs for FEM and the proposed scheme.

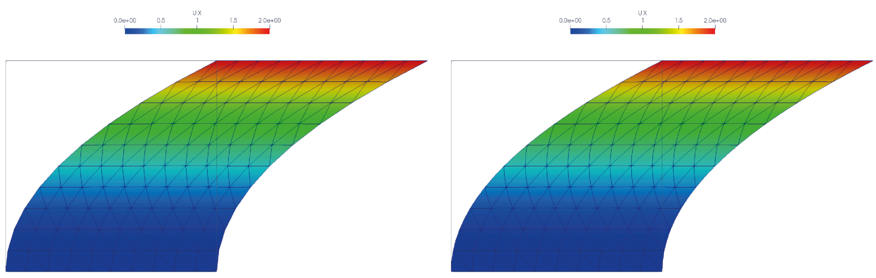

(a) FEM (b) CS-FEM

Figure 9. Current configuration of "Not-so-simple" shear deformation with Dirichlet BCs: (**a**) FEM with T6. (**b**) proposed CS-FEM with T6.

As given in Figure 10a, the displacement error for FEM and proposed CS-FEM is almost identical. The convergence of relative error in strain energy is given in Figure 10b. In this case, the present method is more accurate than FEM.

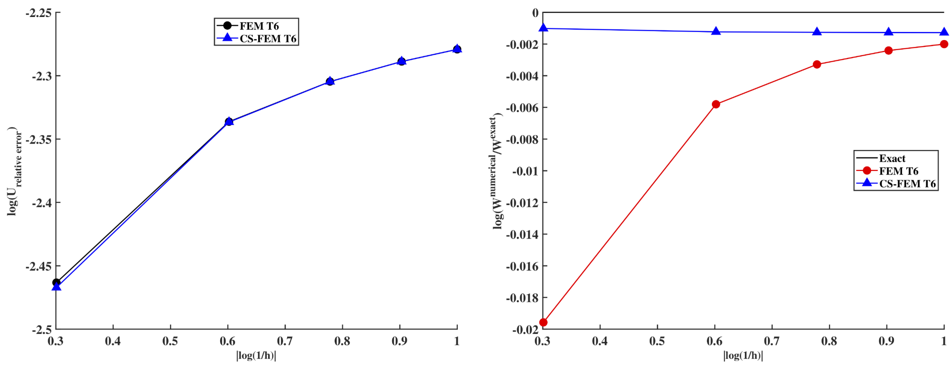

(a) Displacements (b) Strain energy

Figure 10. Convergence of displacements and strain energy relative errors: (**a**) relative error in displacements. (**b**) relative error in strain energy given as $W^{\text{relative error}} = W^{\text{numerical}}/W^{\text{exact}}$.

3.1.4. Bending of a rectangular block

Lastly, an additional non-homogeneous deformation such as bending of a rectangular block is investigated. For this problem, shear modulus $\mu = 0.6$ and bulk modulus $\kappa = 1.95$ equivalent to Poisson's ratio $\nu = 0.36$ are used. The geometry of the block is given in Figure 11.

Preprints (www.preprints.org) | NOT PEER-REVIEWED | Posted: 7 December 2019 doi:10.20944/preprints201912.0091.v1

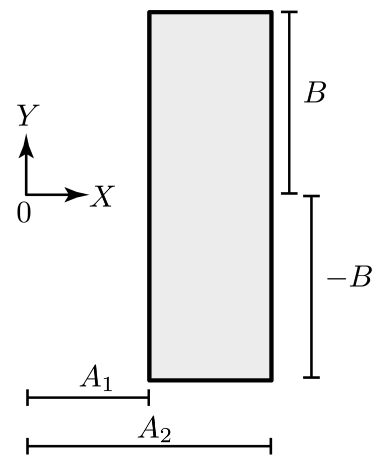

Figure 11. The geometry of the rectangular block for bending test. In this work, the length on x-axis $A = 2$, $A = 3$ and length on y-axis $B = 2$ are used.

For the implementation of Dirichlet BCs, the following cylindrical coordinates in Cartesian coordinates are defined:

$$\begin{aligned} x &= r\cos\theta = \sqrt{2\alpha X}\cos\frac{Y}{\alpha} \\ y &= r\sin\theta = \sqrt{2\alpha X}\sin\frac{Y}{\alpha} \\ z &= 0, \end{aligned} \tag{28}$$

where (x, y, z) are the current Cartesian coordinates and (X, Y, Z) are the initial Cartesian coordinates. Thus the deformation gradient for this test can be obtained as:

$$\mathbf{F} = \begin{bmatrix} f'(X) & 0 & 0 \\ 0 & f(x)\,g'(Y) & 0 \\ 0 & 0 & 1 \end{bmatrix}, \tag{29}$$

where $f(X)$, $g(Y)$, $f'(X)$ and $g'(Y)$ are:

$$\begin{aligned} f(X) &= \sqrt{2\alpha X} \\ f'(X) &= \frac{\sqrt{2\alpha}}{2\sqrt{X}} \\ g(Y) &= \frac{1}{\alpha}Y \\ g'(Y) &= \frac{1}{\alpha}, \end{aligned} \tag{30}$$

where the bending factor $\alpha = 0.9$ is used for this work. Hence, the exact strain energy can be computed as follows:

 doi:10.20944/preprints201912.0091.v1

$$W = \int_2^3 \int_{-2}^2 \left\{ \mu \frac{(0.9 - 2X)^2}{3.6X} \right\} dV \approx 4.485618. \tag{31}$$

Figure 12 illustrates the deformed shapes of the present example for FEM and proposed linear smoothing function scheme. In this study, two cases categorized by different of numbers of elements along each side are used: 1) case 1 is 2×4, 2×8, 2×12, 2×16, 2×20, 2×24, 2×28, 2×32 and 2) case 2 is 4×4, 4×8, 4×12, 4×16, 4×20, 4×24, 4×28, 4×32. When the bending factor α is bigger, the deformed shape becomes a circle as shown in Figure 12.

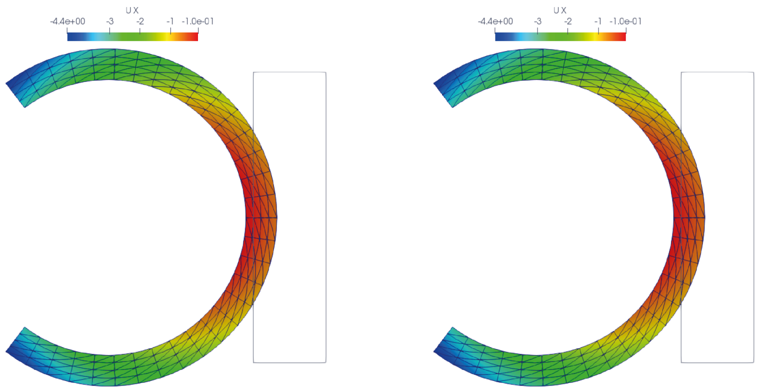

(a) FEM (b) CS-FEM

Figure 12. Deformed shapes of the rectangular block for bending problem: (**a**) FEM with T6. (**b**) CS-FEM with T6.

Figure 13 provides the convergence of displacements and strain energy relative errors in two cases. For both FEM and CS-FEM, relative errors in displacements are almost the same in two cases as shown in Figure 13a. However, the strain energy relative error for the proposed method in two different cases is identical and more accurate than FEM.

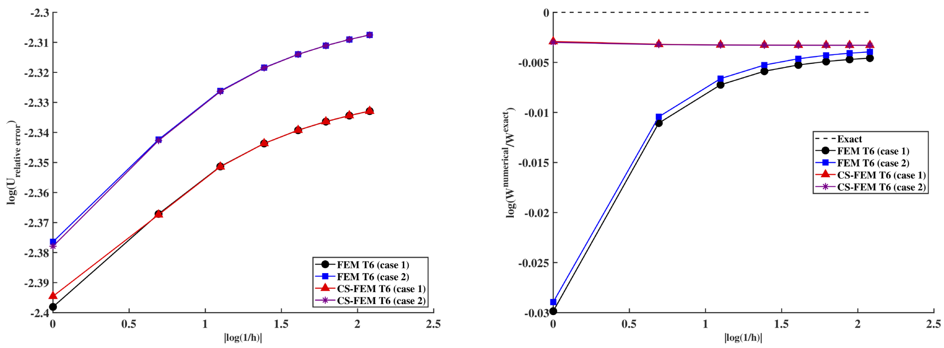

(a) Displacements (b) Strain energy

Figure 13. Convergence of displacements and strain energy relative errors in two cases for bending of the rectangular block: (**a**) relative error in displacements. (**b**) relative error in strain energy given as $W^{\text{relative error}} = W^{\text{numerical}} / W^{\text{exact}}$.

4. Conclusions

In this paper, the linear smoothing function is employed to the cell-based strain-smoothed finite element approximation for the problem of two-dimensional nonlinear hyperelasticity. Unlike the conventional S-FEM, the proposed scheme does not require to the division of finite element cells into sub-cells. Namely, the quadratic triangular element used the smoothing domain itself. Moreover, no further intervention for subdivision is required. Hence, this leads to an increase in the implementation efficiency for the proposed method code. The present CS-FEM with the linear smoothing scheme needs two Gauss points on the boundaries of smoothing domains and three interior Gauss points in the domain. The smoothed strain-displacement matrix is evaluated at the interior Gauss points.

The present CS-FEM is examined by a series of numerical tests to validate its accuracy and stability. The obtained results are compared with the exact solutions. From the results carried out in numerical tests, the following conclusions are obtained: 1) in the homogeneous deformation problem, the proposed CS-FEM with the linear smoothing scheme is able to reproduce machine precision in displacement relative error that is identical to the strain energy relative error and 2) in the non-homogeneous deformation problem, the present scheme shows more accurate results than FEM with fast convergence rate to the exact solution. In future work, the proposed linear smoothing functions to edge-based and node-based strain smoothing approximation will be employed which would effectively handle locking and are less sensitive to distorted meshes than the CS-FEM.

Author Contributions: Conceptualization, C.L. and S.N.; methodology, C.L. and S.N.; software, C.L.; validation, C.L. and S.N.; formal analysis, C.L.; writing–original draft preparation, C.L.; writing–review and editing, S.N.; visualization, C.L.; supervision, S.N.; funding acquisition, C.L.

Funding: This research was funded by National Research Foundation (NRF) of Korea through Ministry of Education under the grant number No. 2016R1A6A1A03012812.

Conflicts of Interest: The authors declare no conflict of interest.

References

1. Liu, G.R.; Dai, K.Y.; Nguyen, T.T. A smoothed finite element method for mechanics problems. *Computational Mechanics* **2007**, *39(6)*, 859–877.
2. Liu, G.R.; Nguyen, T.T.; Dia, K.Y.; Lam, K.Y. Theoretical aspects of the smoothed finite element method (SFEM). *International Journal for Numerical Methods in Engineering* **2007**, *71(8)*, 902–930.
3. Liu, G.R., Nguyen, T.T. *Smoothed Finite Element Methods*, CRC Press: Boca Laton, Florida, USA; 2010.
4. Nguyen-Xuan, H.; Rabczuk, T.; Bordas, S.; Debongnie, J.; A smoothed finite element method for plate analysis. *Computer Methods in Applied Mechanics and Engineering* **2008**, *74*, 175–208.
5. Nguyen-Thanh, N.; Rabczuk, T.; Nugyen-Xuan, H.; Bordas, S.P. A smoothed finite element method for shell analysis. *Computer Methods in Applied Mechanics and Engineering* **2008**, *198*, 165–177.
6. Lee, C.K.; Angela Mihai, L.; Hale, J.S.; Kerfriden, P.; Bordas, S.P.A. Strain smoothing for compressible and nearly-compressible finite elasticity. *Computers & Structures* **2017**, *182*, 540–555.

 doi:10.20944/preprints201912.0091.v1

7. Ong, T.H.; Heaney, C.E.; Lee, C.K.; Liu, G.R.; Nguyen-Xuan, H. On stability, convergence and accuracy of bES-FEM and bFS-FEM for nearly incompressible elasticity. *Computer Methods in Applied Mechanics and Engineering* **2014**, *285*, 315–345.
8. Bordas, S.; Natajaran, S.; Kerfriden, P.; Augarde, C.; Mahapatra, D.; Rabczuk, T.; Pont, T. On the performance of strain smoothing for quadratic and enriched finite element approximations (XFEM/GFEM/PUFEM). *International Journal for Numerical Methods in Engineering*, **2011**, *86*, 673–666.
9. Bordas, S.P.; Rabczuk, T.; Nguyen-Xuan, H.; Nguyen, V.P.; Natarajan, S.; Bog, T.; Quan, D.M.; Hiep, N.V. Strain smoothing in FEM and XFEM. *Computational & Structures* **2010**, *88*, 1419–1443.
10. Jiang, C.; Zhang, Z.Q.; Han, X.; Liu, G.R. Selective smoothed finite element methods for extremely large deformation of anisotropic incompressible bio-tissues. *International Journal for Numerical Methods in Engineering* **2014**, *99(8)*, 587–610.
11. Natarajan, S.; Bordas, S.P.A.; Ooi, E.T. Virtual and smoothed finite elements: a connection and its application to polygonal/polyhedral finite element method. *International Journal for Numerical Methods in Engineering* **2015**, *104*, 1173–1199.
12. Natarajan, S.; Ooi, E.T.; Chiong, I.; Song, C. Convergence and accuracy of displacement based finite element formulation over arbitrary polygons: Laplace interpolants, strain smoothing and scaled boundary polygon formulations. *Finite Elements in Analysis and Design* **2014**, *85*, 101–122.
13. Francis, A.; Ortiz-Bernardin, A.; Bordas, S.P.A.; Natarajan, S. Linear smoothed polygonal and polyhedral finite elements. *International Journal for Numerical Methods in Engineering* **2017**, *109*, 1263–1288.
14. Rand, A.; Gillette, A.; Bajaj, C. Quadratic serendipity finite elements on polygons using generalized barycentric coordinates. *Mechanics of Computations* **2014**, *83*, 2691–2716.
15. Lee, C.K. Gradient smoothing in finite elasticity: near-incompressibility. PhD, Cardiff University, Cardiff, Wales, UK, 2015.
16. Belytschko, T.; Moran, B.; Liu, W.K. *Nonlinear Finite Element for Continua and Structures*; John Wiley & Sons Ltd: Chichester, UK, 2000.